Advanced motor driver for multiple motor configurations

D. Steffensen, H. Johannesen, J. Mejdahl, F. Sanderhoff, R. Eliasen, S. Amstrup

Department of Materials and Production, Aalborg University
Fibigerstraede 16, DK-9220 Aalborg East, Denmark
Email: samstr17@student.aau.dk,
Web page: http://www.mechman.mp.aau.dk/

Abstract
The use of electric motors is an increasing trend in the industry including agricultural livestock ventilation. To keep up with the increasing demands of efficiency and reliability new studies are to be made. One way of increasing reliability is by increasing the number of phases used in a motor. An increased number of phases results in an inherent redundancy, where in most cases one or more phases can fail while the remaining phases are still able to drive the motor on its own. Therefore this paper investigates the possibilities of a versatile multiphase inverter capable of driving several 3-phase induction motors and permanent magnet synchronous motor (PMSM) with up to nine phases. A proof of concept drive is designed and manufactured to be able to take a $400\,\mathrm{V}$ DC input and create nine modulated AC outputs with a maximum total power output of $2.3\,\mathrm{kW}$. Several modes of operations are proposed and tested including driving three 3-phase induction motors with scalar control and a single 9-phase PMSM with FOC. The FOC is implemented with sensorless position feedback through a zero crossing detection algorithm in order to save the cost of one or more encoders. A nonlinear model of the PMSMs are also made and from this, a linear model is derived in order to design controllers for the motor control. The drive was tested and the capability of driving three individual 3-phase induction motors simultaneously with individual speed references at $400\,\mathrm{V}$ was proven. It was further shown that it was possible drive a 3-phase PMSM individually and that it was capable of driving a 9-phase PMSM with FOC at $200\,\mathrm{V}$.

Keywords: PMSM, multiphase motor, FOC, inverter design, versatile inverter

1. Introduction

A variety of different electrical motors are used in the industry for different applications. This also applies for agriculture and livestock ventilation systems, where fans often run for prolonged periods of time in order to keep temperatures suitable for livestock. When dealing with livestock ventilation faulty operation can cause harm to the animals or even entail risk of death. Therefore reliability is a key issue when designing ventilation systems for livestock all over the world. It is desirable to investigate some of the potential benefits of multiphase (more than three phases) motors where redundancy is an inherent feature. When increasing the number of phases in a motor, the redundancy ensures that the motor can continue to operate, even in the case of failure on one or more phases, at the expense of a reduced power output until maintenance is possible[1]. Calculations further shows a possibility of reducing copper losses in PMSM if the number of phases equals half the number of coils in a symmetric stator. This is due to the possibility for a better distribution factor, which entails that all currents can be in phase with the coil EMFs.

Driving a multiphase PMSM requires a drive capable of controlling several phases simultaneously, and since a multiphase PMSM is not a standard motor, such drives are not commercially available to the knowledge of the authors. Therefore this paper focuses on the design of a versatile 9-phase drive. Since the phases in a 9-phase motor drive can be controlled individually, it is also capable of driving three 3-phase motors. It is therefore desired to design a drive that can control a variety of different motors and thereby possibly making it commercially more interesting. This includes three 3-phase induction motors (IM), three 3-phase PMSMs or one 9-phase PMSM. In order to efficiently drive the PMSMs it is decided to implement Field Oriented Control (FOC).

2. Printed circuit board design

The following section treats the design of the inverter shown in Figure 1. Due to the low dynamic requirement of livestock ventilation, it is desired to further reduce costs by implementing sensorless FOC and thereby save the cost of an encoder.

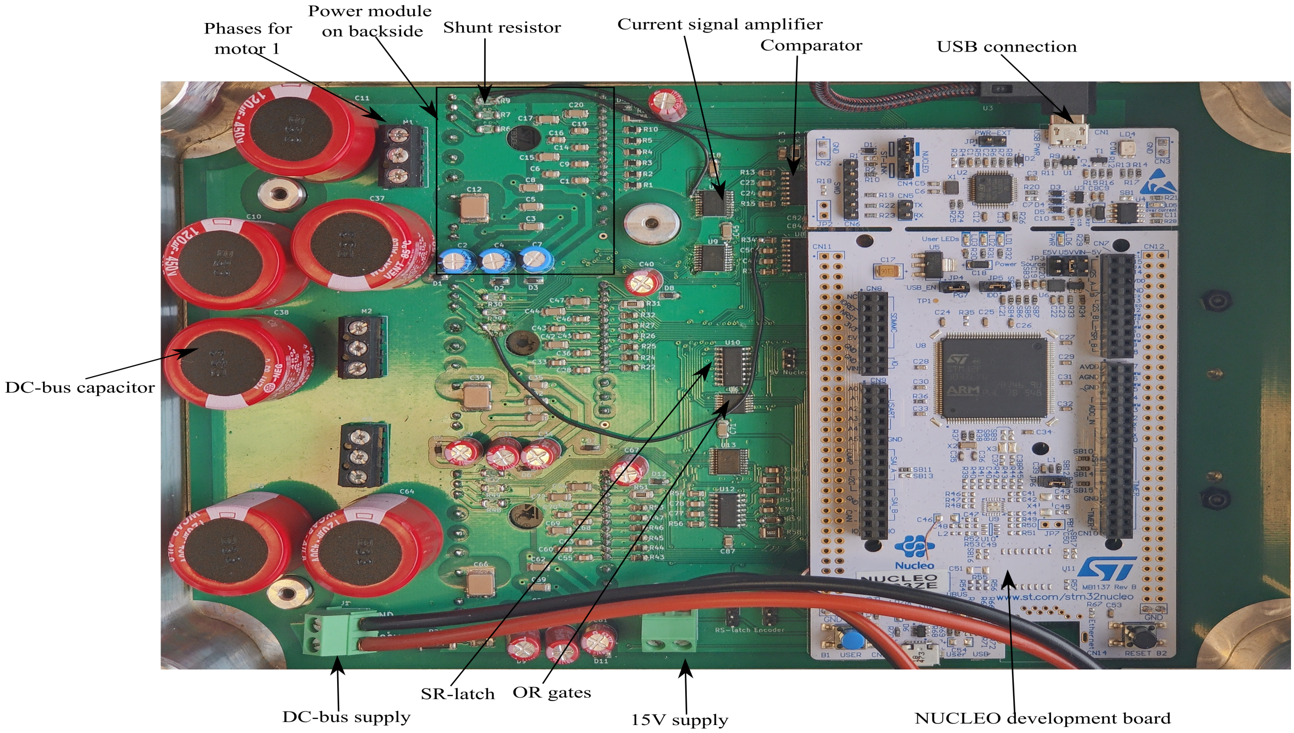

Fig. 1 The figure shows the proof-of-concept inverter with labels on central components.

2.1 Hardware requirements

In order to achieve the desired functionalities of the inverter, the following requirements are listed for the hardware, which must be able to:

- Operate with a 400 V DC supply.
- Handle 2.3 kW input power from DC supply.
- Fit inside a specific aluminium box.
- Support sensorless drive of:
  - One 9-phase PMSM.
  - Three 3-phase PMSMs.
  - Three 3-phase IM.
- Operate with ambient temperatures between 0 °C and 40 °C.
- Operate exclusively with passive cooling.

2.2 Software requirements

The software and implemented controllers must be able to:

- Have a switching frequency of 5 kHz.
- Execute the code with at least the switching frequency .
- Control either one of the following.
  - One 9-phase PMSM with FOC.
  - Three 3-phase PMSM with FOC.
  - Three 3-phase IM with scalar control.
- Support the required hardware functionalities.
  - DC-bus voltage measurement.
  - Current measurements on all phases.
- Drive the motor with a range between 0 and 1000 RPM.

It is worth noting, that a fan application has low dynamic requirements, as the settling time is of less importance. Instead the dynamic requirements of the electrical and mechanical are specified in accordance to the switching frequency. Here the desired bandwidth of the systems are determined for the electrical and mechanical system as 1/20 and 1/200 of the switching frequency, respectively.

2.3 Hardware design

The inverter contains two central components and a number of auxiliary components and circuits. The central components are a microcontroller unit (MCU) and several 3-phase power modules. As described in section 2.1, it is necessary to design an inverter, that can output nine individual phases, and therefore 3 power modules are needed. The printed circuit board (PCB) design is based on three standard power modules (STIB1060DM2T-L) that has three half bridges each. In this way it is possible to drive the power modules individually in order to control three separate 3-phase motors or drive the modules together in order to control a single 9-phase motor.

A NUCLEO-F303ZE development board is chosen as the MCU since it, among other features, has three dedicated motor control timers, a $72\,\mathrm{MHz}$ clock speed and 4 ADCs. It is thereby able to drive the three power modules on an individual basis, but since the timers can be synchronised, it is also able to drive the three power modules together. The current in all phases are measured through a low side shunt resistor creating a voltage difference according to Ohm's law. The resistance of the shunt resistors are kept low at $25\,\mathrm{m\Omega}$ in order to minimize losses, which entails current signals in the mV range. These signals are gained by a factor of 20 through operational amplifiers (op-amps), see Figure 1, and the full scale resolution of the ADC can thereby be utilised.

Trace distances and widths are designed in accordance with at least the minimum conductor spacing specified in IPC-2221. The PCB is designed to separate high voltage and current traces from low voltage and current traces, in order to reduce the induced noise on the measurement and control signals. The left side of the PCB is designated to high currents and voltages, as the right part of the PCB in Figure 1 is designated to low voltages and currents.

3. Time domain model

An electrical time domain model is derived for a general n-phase PMSM in order to design suitable controllers for both 3-phase and 9-phase motors. Both models are derived based on the models in [2] and [3]. All phases can be modeled as an applied voltage, voltage drop over a resistor, voltage drop due to a change in flux linkage and the back electromotive force (EMF) as shown in Figure 2.

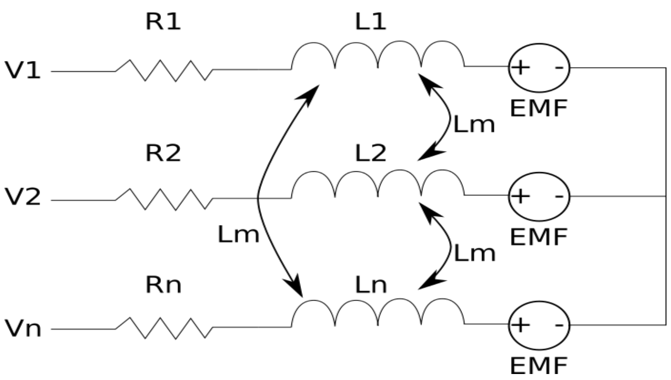

Fig. 2 Schematic of the motor modeled as n phases with a resistance, an inductance, a mutual inductance and a back EMF.

3.1 Electrical model

The system can be simplified significantly by the following assumptions:

- All phases has the same resistance and inductance independent of position
- Magnetic saturation, and temperature dependencies are neglected
- The back EMF and magnetomotive force are sinusoidal, i.e. no harmonics

When applying these assumptions, the set of equations can be written in a compact matrix form:

$$[v] = [R]\,[i] + \frac{d}{dt}\left([\psi] + [\psi_{pm}]\right) \tag{1}$$

Where the vectors $[i]$, $[R]$, $[i]$, $[\psi]$ and $[\psi_{pm}]$ respectively stand for terminal phase to neutral voltage, phase winding resistance, phase current, phase flux linkage and flux linkage from the permanent magnets. $[R]$ is a diagonal matrix of size n x n with the phase resistance as the diagonal elements. When all resistances are assumed equal, the matrix can be reduced to a scalar value. The vectors are defined as follows:

$$[v] = \begin{bmatrix} v_1 & v_2 & v_3 & \dots & v_n \end{bmatrix}^t \tag{2}$$

$$[i] = \begin{bmatrix} i_1 & i_2 & i_3 & \dots & i_n \end{bmatrix}^t \tag{3}$$

$$[\psi] = \begin{bmatrix} \psi_1 & \psi_2 & \psi_3 & \dots & \psi_n \end{bmatrix}^t \tag{4}$$

$$[\psi_{pm}] = \begin{bmatrix} \psi_{pm1} & \psi_{pm2} & \psi_{pm3} & \dots & \psi_{pmn} \end{bmatrix}^t \tag{5}$$

Where the phase flux linkage and flux contribution from the permanent magnets can be seen below.

$$[\psi] = [L][i] \tag{6}$$

$$[\psi_{pm}] = \lambda_{pm}[\gamma_n] \tag{7}$$

The amplitude of the permanent magnet flux linkage is given by λ_{pm}, which is a scalar constant, while γ_n is position and phase dependent and α_e is the electrical angle between phases, as described in:

$$[\gamma_n] = [\ \cos(\theta_e) \quad \cos(\theta_e - \alpha_e) \quad \cos(\theta_e - 2\alpha_e) \quad \dots \quad \cos(\theta_e - n\alpha_e)\ ]^t \tag{8}$$

The inductance matrix shown in Equation 6 contains self inductance and mutual inductance from all phases:

$$[L] = \begin{bmatrix} L_{11} & L_{12} & L_{13} & \dots & L_{1n} \\ L_{21} & L_{22} & L_{23} & \dots & L_{2n} \\ L_{31} & L_{32} & L_{33} & \dots & L_{3n} \\ \dots & \dots & \dots & \dots & \dots \\ L_{n1} & L_{n2} & L_{n3} & \dots & L_{nn} \end{bmatrix} \tag{9}$$

The self inductances for each phase can be seen on the diagonal in Equation 9. Since the inductance in all phases are assumed equal, $L_{11} = L_{22} = ... = L_{nn}$ is true. The self inductance can also be described as $L_{nn} = L_l + M$, where L_l is the leakage inductance and M is the working inductance that links to the rotor. The off-diagonal entries represents the mutual inductance. It can be proven that for a symmetrical motor, there will be $(n-1)/2$ different values of mutual inductance. These can be calculated as [2]:

$$L_{mi} = M\cos(i\alpha_m),\ i \in \{1, 2, \dots, (n-1)/2\} \quad (10)$$

Where α_m is the mechanical angle between phases.

3.2 Transformations

The above derived model is valid in the stator fixed natural reference frame. When controlling a PMSM it is advantageous to control it in a different reference frame than the natural n-phase frame, where voltages and currents are sinusoidal. By transforming the system into a rotor fixed reference frame, voltages and currents becomes DC values in steady state, which eases the control. Figure 3 shows the three reference frames used in the transformation. This illustration is based on a 3-phase system, but it can easily be expanded to n phases, where additional phase axes appears.

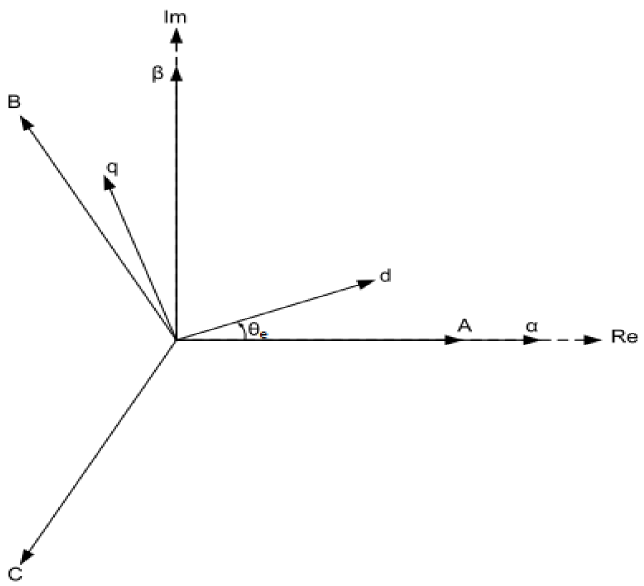

Fig. 3 The three different reference frames used in the transformation [3].

3.2.1 Clarke transformation

Under the assumption of a balanced sinusoidal input the Clarke transformation can be used to transform an arbitrary number of phases in the natural reference frame into a two-dimensional stator fixed reference frame called $\alpha\beta$ [2]. In general it can be expressed as:

$$[f]_{\alpha\beta} = \sqrt{\frac{2}{n}} \cdot [C]\,[f_{1,2,\dots n}] \quad (11)$$

Where $[C]$ is the Clarke transformation matrix, that has n columns, $[f_{1,2,\dots n}]$ is values in the n-phase natural reference frame and $[f]_{\alpha\beta}$ is the same values converted into the $\alpha\beta$ reference frame. The factor $\sqrt{2/n}$ in front of the matrix in Equation 11 is to ensure that the total power of the original machine remains invariant under the transformation.

$$[C] = \begin{array}{c} \alpha \\ \beta \end{array} \begin{bmatrix} 1 & \cos\alpha_e & cos2\alpha_e & \cdots & cos2\alpha_e & cos\alpha_e \\ 0 & \sin\alpha_e & \sin 2\alpha_e & \cdots & -\sin 2\alpha_e & -\sin\alpha_e \end{bmatrix} \quad (12)$$

The matrix shown in Equation 12 is a reduced form, where it is assumed that the motor is balanced and there is no harmonics. If these assumptions are not valid more rows will be included in the matrix. When applying the Clarke transformation in Equation 11 to the model in the natural stator fixed reference frame, Equation 1, it can be seen, that the n equations is reduced to the following two equations:

$$v_\alpha = Ri_\alpha + L_{eq}\frac{di_\alpha}{dt} + \lambda_{pm}\sqrt{\frac{2}{n}}[C_\alpha]\left(\frac{d}{dt}[\gamma_n]\right) \quad (13)$$

$$v_\beta = Ri_\beta + L_{eq}\frac{di_\beta}{dt} + \lambda_{pm}\sqrt{\frac{2}{n}}[C_\beta]\left(\frac{d}{dt}[\gamma_n]\right) \quad (14)$$

Where $[C_\alpha]$ and $[C_\beta]$ are the α and β rows in Equation 12. This reduction in the number of equations is done without loss of information, as long as the supplied voltage is a balanced symmetrical n-phase sinusoidal supply [2].

3.2.2 Park transformation

During steady state operation of a PMSM, α and β voltages and currents have a sinusoidal wave form. The Park transformation is capable of transforming the stator fixed $\alpha\beta$-model into a rotor fixed dq-model, where the d and q axis voltages and currents are DC-values during steady state operation. The DC-values of d and q voltage/current makes it an optimal reference frame to perform the control in. The general form of the Park transformation can be written as:

$$[f_{dq}] = [D]\,[f_{\alpha\beta}] \quad (15)$$

Where:

$$[D] = \begin{array}{c} d \\ q \end{array} \begin{bmatrix} \cos\theta_e & \sin\theta_e \\ -\sin\theta_e & \cos\theta_e \end{bmatrix} \quad (16)$$

In the case, where the supplied voltage is not balanced and symmetrical, and the Clarke transform contains more than just the α and β values, the D-matrix is expanded with ones on the diagonal and zeros one the off-diagonal until it matches the Clarke transform.
The result of the Park transform becomes:

$$v_d = Ri_d + \frac{d\psi_d}{dt} - \omega_e\psi_q \tag{17}$$

$$v_q = Ri_q + \frac{d\psi_q}{dt} + \omega_e\psi_d \tag{18}$$

Where $\psi_d = L_d \cdot i_d + \lambda_{pm}$ and $\psi_q = L_q \cdot i_q$. From Equation 17 and 18 it can be seen that the system works with DC values, which simplifies the job of the controller. It is worth noting that due to the magnetic permeability of magnets being close to the permeability of air, $L_d \approx L_q \approx L$ and thereby assumed constant for surface mounted PMSMs.
The electromechanical torque can be expressed as:

$$\tau_e = \frac{9p}{4}\lambda_{pm}i_q \tag{19}$$

Where p is the number of poles.

3.3 Mechanical model

The mechanical model is based on Newton's second law where:

$$J_m\frac{d\omega_m}{dt} = \tau_e - \tau_m \tag{20}$$

$$\tau_m = B_m\omega_m + \tau_{df} + \tau_L \tag{21}$$

The dry friction, τ_{df}, is assumed so to be negligible and the fan load is modeled as a quadratic load:

$$\tau_L = K_f\omega_m^2 \tag{22}$$

This load model does not account for changes in the load caused by wind gusts or the like. The full mechanical model then becomes:

$$J_m\frac{d\omega_m}{dt} = T_e - T_m = \frac{9p}{4}\lambda_{pm}i_q - (B_m\omega_m + K_f\omega_m^2) \tag{23}$$

3.4 Linearisation

The model equations for the electric system found in Equation 17 and 18 and the mechanical Equation 23 are restated below:

$$\frac{di_d}{dt} = \frac{1}{L}\left(u_d - Ri_d + L\omega_e i_q\right) \tag{24}$$

$$\frac{di_q}{dt} = \frac{1}{L}\left(u_q - Ri_q - L\omega_e i_d - \lambda_{pm}\omega_e\right) \tag{25}$$

$$\frac{d\omega_m}{dt} = \frac{1}{J_m}\left(\frac{3p}{4}\lambda_{pm}i_q - B_m\omega_m - K_f\omega_m^2\right) \tag{26}$$

It can be seen in the equations above that none of them are linear by nature. The two electric equations, Equation 24 and 25, has cross couplings in the terms $L\omega_e i_q$ and $-L\omega_e i_d$, while $\lambda_{pm} \cdot \omega_e$ is velocity dependant. MIMO system control could be utilized in order to handle the cross couplings. However due to the low dynamic requirements of a ventilation application a SISO system controller is assessed to be sufficient. A simplistic approach to linearisation of the electrical system is to disregard the cross couplings, discussed above and treat them as disturbances. This can be done since the terms primarily has an effect on transient responses at high rotational speeds. The ventilation application only has transient operation during startup, whereof a large part of the startup operation will be at low rotational speeds. The back EMF term, $\lambda_{pm}\omega_e$, is also considered as a disturbance, since the changes in current will have a much faster dynamic response than the back EMF. This leaves the following electrical transfer functions:

$$G_{ed}(s) = \frac{i_d}{u_d} = \frac{1}{Ls + R} \tag{27}$$

$$G_{eq}(s) = \frac{i_q}{u_q} = \frac{1}{Ls + R} \tag{28}$$

Since $G_{ed}(s) = G_{eq}(s)$ the electrical system is reduced and denominated to two $G_e(s)$ systems.

The nonlinear load term of the mechanical model, Equation 26, can be linearised with a first order Taylor expansion:

$$K_{f.lin} = \frac{\partial\tau_L(\omega_{m0})}{\partial\omega_m} = 2K_f\omega_{m0} \tag{29}$$

Which gives the following linearized load:

$$\tau_{fan.lin} = K_{f.lin} \cdot \Delta\omega_m \tag{30}$$

When the nonlinear term is replaced with the linearised Taylor approximation, the following transfer function is obtained:

$$G_{me}(s) = \frac{3p}{4}\lambda_{pm}\frac{1}{J_m s + (B_m + K_{f.lin})} \tag{31}$$

3.5 Motor parameters

The motor parameters are determined for the 9-phase PMSM, which is configured as shown in Figure 4. Here $A1$ and $A1'$ are connected in series and labeled as phase $A1$, $A2$ and $A2'$ are connected in series and so forth.

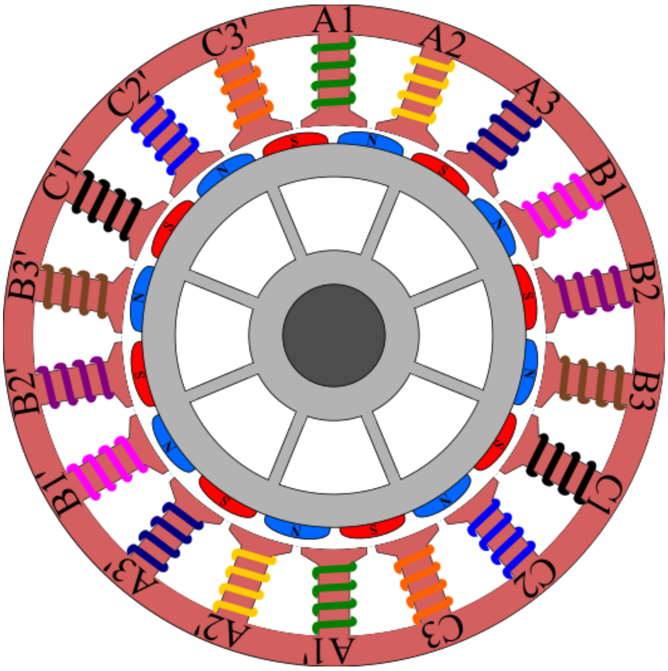

Fig. 4 Windings in 9-phase configuration, where coils of the same color is in series connection.

3.5.1 Inductance

The phase inductance is measured with a Kerr Precision Magnetics Analyzer in the laboratory and is found to be $L_{phase} = 24\,\text{mH}$.
Assuming there is no leakage inductance, the mutual inductances can be calculated with Equation 10. Entering these values into Equation 9 yields the inductance matrix in the natural reference frame. In order to transform these inductances into the dq reference frame, the following steps are conducted. The inductance matrix can be diagonalized with the total transformation matrix [4], [2]:

$$[T] = [D]\sqrt{\frac{2}{n}}[C] \tag{32}$$

$$L_{diag} = [T][L][T]^{-1} \tag{33}$$

The first two diagonal entries in L_{diag} is the d- and q-axis inductances used in the controller design and the model. This value is found to be $L_{d9} = L_{q9} = 108\,\text{mH}$

3.5.2 Flux linkage amplitude

The flux linkage amplitude parameter, λ_{pm}, can be described by [2]:

$$\lambda_{pm} = \frac{k_w N}{2}\phi_p \tag{34}$$

$$\phi_p = B_g \frac{\pi D L_{stk}}{2P} \tag{35}$$

Where k_w is the winding factor, N is the effective number of turns on the coils in a phase, B_g is the pole flux density in the air gap, D is rotor diameter, L_{stk} is the length of the stack and P is the number of pole pairs. Using these equations gives a flux linkage amplitude of $\lambda_{pm9} = 0.222\,\frac{\text{V}}{\text{rad/s}}$.

3.5.3 Stator resistance

The resistance of each coil is measured and the average coil resistance is found to be $R_{avg} \approx 0.87\,\Omega$ with exception from coil C3' a maximum deviation of $0.09\,\Omega$. Coil C3' has a resistance of $1.45\,\Omega$ which is assessed to be due to either a manufacturing error or a cold solder joint.

3.5.4 Inertia

Based on the information in the motor datasheet, the moment of inertia is found to be $J_{rotor} = 4.358 \times 10^{-3}\,\text{kg}\cdot\text{m}^2$.
The fan consists of three blades each weighing $0.75\,\text{kg}$ with a length of $0.75\,\text{m}$. The hub has a diameter of $0.2\,\text{m}$ and a weight of $1\,\text{kg}$. Assuming the blades to be homogeneous the moment of inertia is calculated as:

$$J_{tot} = 0.43\,\text{kg}\cdot\text{m}^2 \tag{36}$$

3.5.5 Viscous friction

A viscous friction coefficient, B_m is found to be $4.67 \times 10^{-4}\,\frac{\text{Nm}\cdot\text{s}}{\text{rad}}$ in the datasheet from the motor.

4. Control strategy

Different control strategies are utilized for driving IMs and PMSMs. The IMs are controlled with a simple scalar control based on the rated motor voltage and rated frequency. The control strategy used to control the PMSM is FOC. This allows for direct control of the flux producing current and the torque producing current. Implementation of FOC in 3-phase systems are well described in literature and many examples can be found. FOC of 9-phase systems however, is not as well documented in literature and when described, several different approaches are proposed. This paper investigates the opportunity of controlling the PMSM as if it consisted of three individual symmetric 3-phase systems and thereby dividing the calculation into three 3-phase dq-systems as shown in Figure 5. In that way phase $A1$, $B1$ and $C1$ from Figure 4 is collected as Set 1 in Figure 5. The three symmetrical coil sets have a 20° mechanical offset and therefore the 8 pole pairs means that the coil sets have a 160° electrical offset. This means the angles, θ_{e1}, θ_{e2} and θ_{e3} on Figure 5

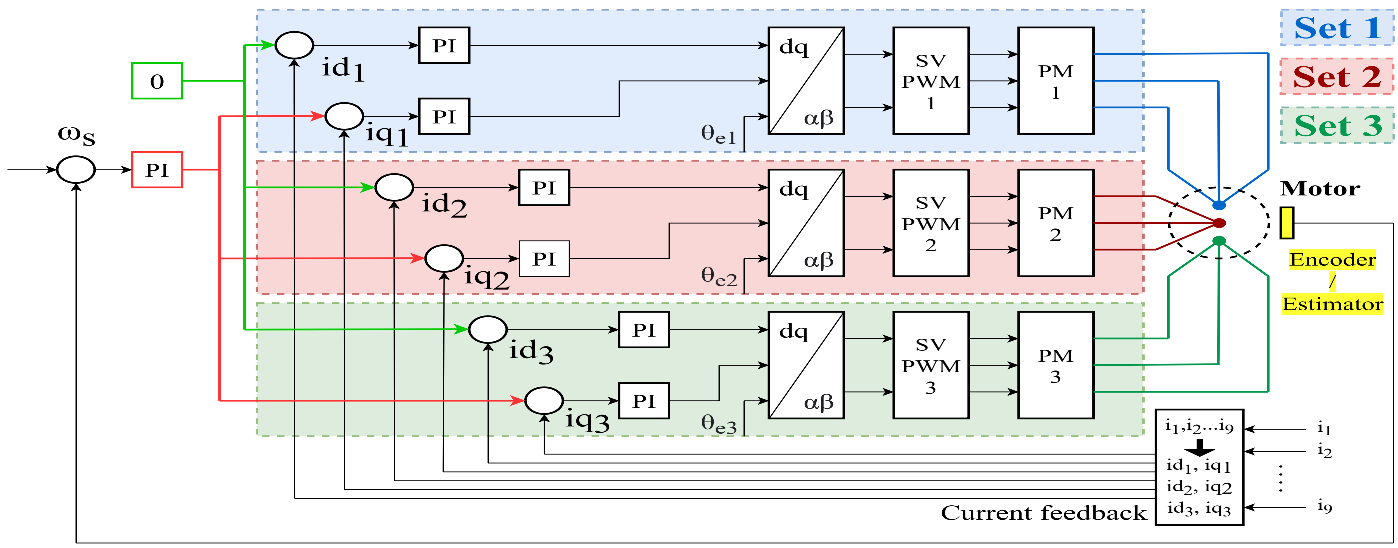

Fig. 5 FOC strategy for 9-phased system.

have a 160° offset.

Utilizing three dq-systems entails a slightly more robust system, since unbalances in the system in terms of inaccuracies, parameter variation or environmental factors can be controlled on a lower level, as it is possible to control three d and q currents instead of just one. However, it has to be noted, that the three systems would be coupled, due to the mutual inductance between the phases. Dividing the system into 3 symmetric subsystems also results in an inherent fault tolerance. The system will continue to operate if the phases on two of the power modules fail or even one or two of the power modules have open circuit fails, since the three subsystems operate independently, though there will be a reduced torque and power output.

4.1 Position estimation

Both the Park transformation and the inverse Park transformation needs position feedback from the rotor, which can be determined with several different methods. The standard method is the use of an encoder mechanical attached to the rotor shaft. However for low dynamic applications, a sensorless zero crossing estimation algorithm can be used to estimate the position, and thereby reduce expenses associated with an encoder. The zero crossing estimation algorithm is based on a rearranged form of Equation 1 transformed into $\alpha\beta$-reference frame:

$$e_\alpha = v_\alpha - Ri_\alpha - L_{eq}\frac{di_\alpha}{dt} \tag{37}$$

By estimating the zero crossings of the back EMF and interpolating between them, the rotor position can be estimated. Since the time derivative of the phase current is a part of the equation input, a first order filter is designed to reduce noise on the output from the numerical differentiation. This method is not well suited for low velocity application, since the back EMF must be of a significant size, in order to have a useful signal to noise ratio. It is further worth noting, that this method only finds the correct position as long as the speed is constant, and it is therefore best suited for applications with low dynamics such as ventilation.

4.2 Controller design

As shown in Figure 6, the control of the system is done with a cascade control structure, where the current controller is designed with a bandwidth high enough so that it can be neglected during the design of the speed controller. The controller design is based on a procedure described by [5]

4.2.1 Current controller

For the current controller, a PI-controller is used to obtain a pole-zero cancellation of the electrical system. The standard PI-controller can be rearranged as:

$$G_{ce}(s) = K_{pe}\left(1 + \frac{1}{T_i s}\right) = K_{pe}\frac{s + \frac{1}{T_i}}{s} \tag{38}$$

Where $T_i = \frac{K_{pe}}{K_{ie}}$. It can be seen that Equation 38 consists of a zero and a free integrator, where the gains can be chosen such that the zero of the controller cancels the pole of the electrical system. Applying the controller

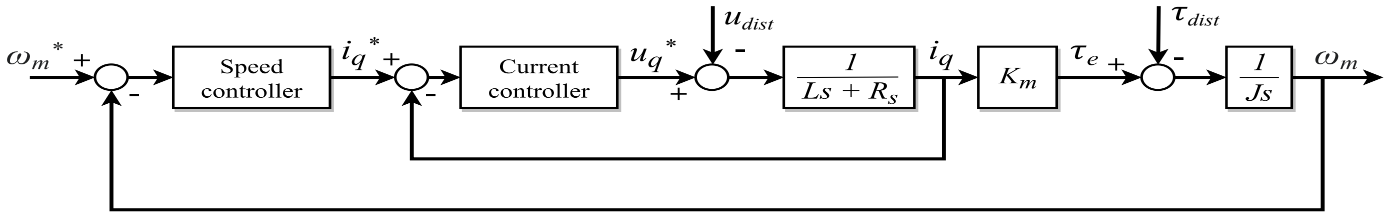

Fig. 6 Cascade control structure (only q-axis system is shown.)

to the electrical system gives the following:

$$\begin{aligned} G_{ec}(s)G_e(s) =& K_{pe}\frac{s+\frac{1}{T_i}}{s}\cdot\frac{1}{Ls+R_s} \\ =& K_{pe}\frac{s+\frac{1}{T_i}}{s}\cdot\frac{\frac{1}{L}}{s+\frac{R_s}{L}} \end{aligned} \tag{39}$$

It can be seen that the pole zero cancellation is achieved when:

$$\frac{1}{T_i} = \frac{K_{ie}}{K_{pe}} = \frac{R_s}{L} \tag{40}$$

And thereby reducing the system to:

$$G_{ec}(s)G_e(s) = \frac{1}{\frac{L}{K_{pe}}s} \tag{41}$$

The cros-over frequency can be found as:

$$\begin{aligned} |G_{ec}(j\omega_{co})G_e(j\omega_{co})| =& \frac{1}{|\frac{L}{K_{pe}}j\omega_{co}|} = 1 \\ \implies \quad \omega_{co} =& \frac{K_{pe}}{L} \end{aligned} \tag{42}$$

According to [5], the bandwidth of the closed loop equals the cross-over frequency of the open loop response. Therefore Equation 40 and 42 gives:

$$\begin{aligned} K_{pe} &= L\cdot\omega_{bwc} \\ K_{ie} &= \frac{R_s}{L}K_{pe} = R_s\cdot\omega_{bwc} \end{aligned} \tag{43}$$

It is shown that the current controller can be designed for pole-zero cancellation based on motor parameters and a desired bandwidth. According to currentcontrol, a rule of thumb is to set the bandwidth for the current controller to 1/20 of the switching frequency, $\omega_{bwc} = 5000\,\mathrm{Hz}/20 = 250\,\mathrm{Hz}$.

4.2.2 Speed controller

The speed system can be expressed as consisting of the speed controller, the closed loop electrical system, and the mechanical system.

$$G_s(s) = G_{cs}(s)G_{cle}(s)G_{me}(s) \tag{44}$$

Where the closed loop electrical system is significantly faster than the mechanical system and thereby $G_{cle} \approx 1$.

$$G_s(s) \approx K_{ps}\frac{K_m}{J_m s} \tag{45}$$

Equation 45 is true, as long as the cutoff frequency of the speed controller has a significantly lower value than the cross-over frequency of the mechanical system. The controller for the resulting system can be designed in a similar way as the current controller to obtain pole-zero cancellation. It can be shown that:

$$\omega_{bws} = \frac{K_{ps}K_m}{J_m} \tag{46}$$

As long as the controller corner frequency is sufficiently lower than the cross-over frequency of the system [5]. The corner frequency of the PI-controller is defined as:

$$\omega_{cs} = \frac{K_{is}}{K_{ps}} \tag{47}$$

When Equation 45 and 47 is combined, the following is obtained:

$$K_{ps} = \frac{J_m}{K_m}\omega_{bws} \tag{48}$$

According to [5], the corner frequency of the controller should be placed approximately a decade lower than the cross-over frequency of the system:

$$\omega_{cs} = \frac{\omega_{com}}{10} \Leftrightarrow K_{is} = K_{ps}\frac{\omega_{com}}{10} \tag{49}$$

Where ω_{com} is the cross-over frequency of the mechanical system. Thereby the speed controller is designed, based on the system parameters, to be:

$$G_{cs} = \frac{J_m}{K_m}\omega_{bws} + \frac{K_{ps}\frac{\omega_{bws}}{10}}{s} \tag{50}$$

Where the speed system bandwidth should be 10 times lower than the bandwidth of the current system [5], $\omega_{bws} = \frac{250\,\mathrm{Hz}}{10} = 25\,\mathrm{Hz}$. Both the current and speed controller is discretized with Tustin's method and implmented on the microcontroller together with an integrator anti-windup.

5. Test and results

5.1 Three 3-phase induction motors

A test with three individual IMs was carried out as shown in Figure 7, where three 3-phase IMs are driven with a 400 V DC-bus. The onboard electronics on the inverter are powered by the 15 V power supply shown on Figure 7. The IMs are controlled with scalar control,

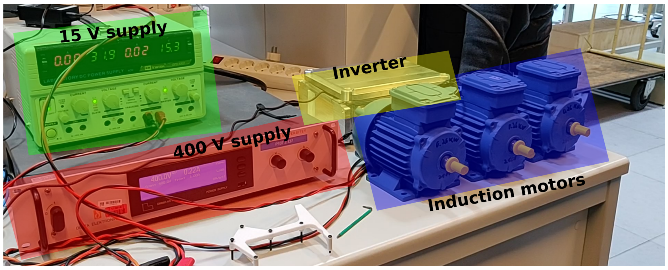

Fig. 7 The test setup with three 3-phase IMs.

where the voltage and frequency relationship is kept constant and based on the rated voltage and frequency of the motors. A modulated sinusoidal AC voltage output is applied. If the control and modulation is implemented correctly, sinusoidal currents should appear in the motor, and the rotor should be spinning. This is also the case as shown in Figure 8.

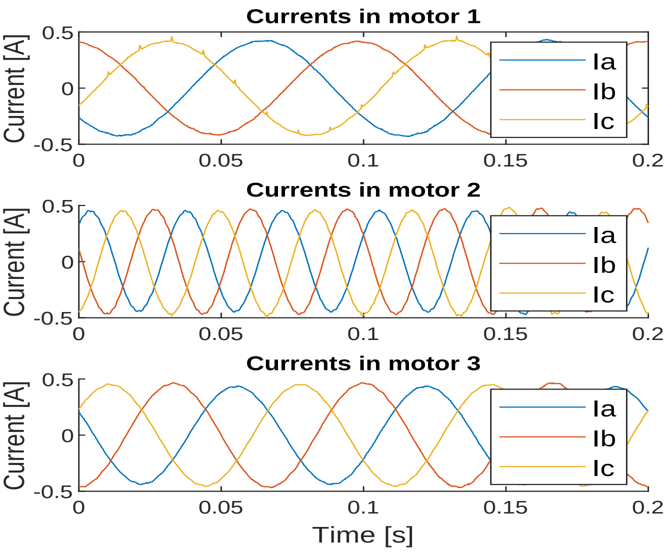

Fig. 8 Data showing the currents while driving IMs.

Figure 8 shows the currents, measured by the MCU, during the test with three 3-phase IMs. The different frequencies is a consequence of different speed references on the individual motors and thereby different speeds on the output shaft. It can also be seen that the sequence is different from motor 1 and the two other motors, where the phases of motor one peak in a 'A,B,C' sequence and the two others has a 'A,C,B' sequence. This is caused by the fact, that motor one is set to rotate clockwise, while the two other motors are set to rotate counterclockwise. Phase C in motor 1 on Figure 8 has periodic spikes as the only phase. An external wire is soldered on the current measurement circuit on phase C1, in order to correct a hardware mistake. It is suspected, that this wire is more susceptible to noise.

5.2 PMSM

In order to verify the performance of the drive, several tests with 3-phase and 9-phase PMSMs are conducted.

5.2.1 3-phase PMSM

The 3-phase PMSM test is conducted in order to ensure, that the microcontroller is properly configured and to validate the functional performance of the position estimator. The test is conducted with a 60 V, 0.5 A limited power supply, in order to protect the hardware in case of system failure. Several tests are conducted, where the 3-phase PMSM is tested on the three different power modules one after another. In order to validate the position estimator, the estimated position is compared to the signal from an encoder mounted on the PMSM. The tests showed similar results regardless of the used power module. Therefore only the test data from one of the test are shown in Figure 9. The currents seen in Figure 9 are

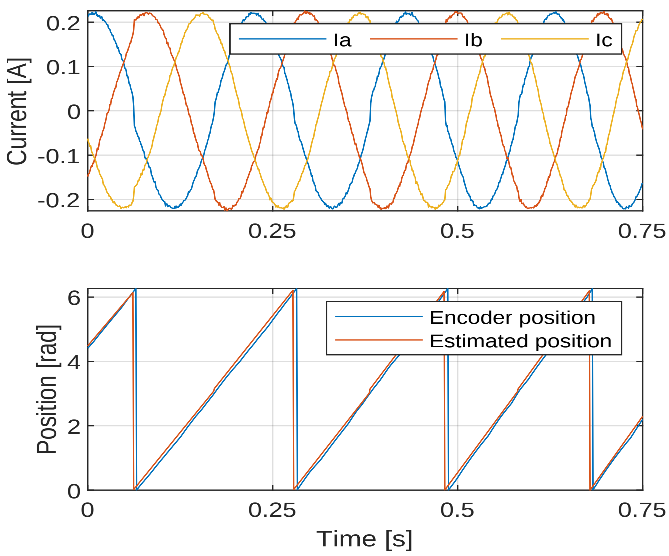

Fig. 9 Data showing the currents and position of the 3-phase PMSM.

approximately sinusoidal, while the estimated position is very close to the position found by the encoder. Small notches is noticed in the currents twice every period. These are caused by the position being updated at these instants and therefore an instant change is made in the dq-frame which leads to a change in the applied

voltages.
Based on this it is concluded that both hardware and software is ready for a high voltage 9-phase test.

5.2.2 9-phase PMSM

The 9-phase PMSM test aims to validate that the drive is capable of driving a 9-phase PMSM with a DC-bus of 400 V. Several tests were conducted starting with a 60 V DC-bus and then gradually increase the voltage after each test. During the tests a fan was mounted on the PMSM and the motor was securely strapped to a test bench. During the test, different electromagnetic noise related problems arose, and it was not possible to conduct tests where the DC-bus voltage exceeded 200 V. Increasing the DC-bus voltage above 200 V resulted in loss of data in the communication between the microprocessor and computer, and even random restarts of the microprocessor. The data from the 200 V test is shown below: The data seen in Figure 10

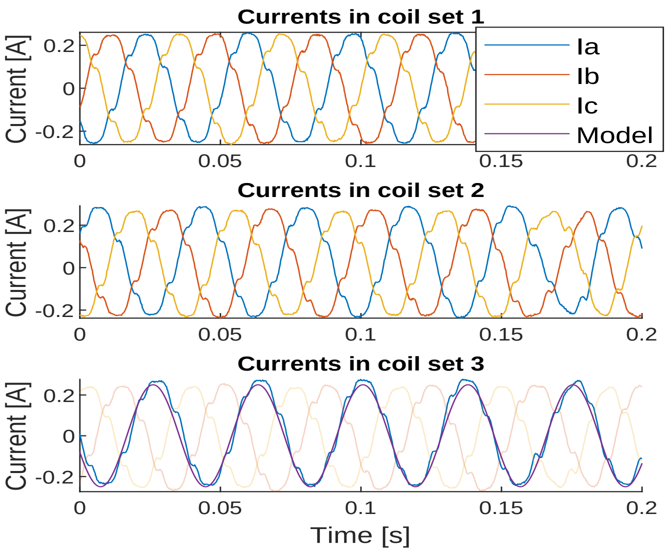

Fig. 10 Data showing the currents in all nine phases during the 200 V test.

shows somewhat sinusoidal currents, but with periodic plateaus. It is suspected, that these plateaus are a result of the more complex couplings in the 9-phase motor. However these data does not reveal why the high amount of noise was present at higher DC-bus voltage. It is suspected that the cable routing is a partly responsible of the noise. The galvanically isolated USB adapter used between microprocessor and computer could also be less noise tolerant than a directly coupled connection between the two.
From the 9-phase PMSM test it can be concluded that the designed drive is capable of driving a 9-phase PMSM with up to 200 V on the DC-bus. It is also suspected that further testing and electromagnetic noise countermeasures, could make it possible to drive a 9-phase PMSM with up to 400 V on the DC-bus. The model data seen in coil set 3 in Figure 10 has almost the same frequency and amplitude as the measured data. Therefore the model is deemed sufficiently accurate.

6. Conclusion

A versatile motor drive, capable of driving three 3-phase IMs, three 3-phase PMSM or one 9-phase PMSM, has successfully been designed, produced and tested. The inverter shows good results when driving three 3-phase IMs with scalar control.
The control strategy with the three separate dq-systems for FOC of PMSMs is implemented in a way that allows for two different modes of PMSM operation, three 3-phase PMSMs or one 9-phase PMSM. This implementation results in redundancy when driving the 9-phase machine, since it is based on three separate system, that can operate regardless of whether the other systems are connected or not. In case of failure of one or more phases or power modules, the remaining power module(s) is capable of driving the PMSM though with reduced power output.
The test of the 9-phase PMSM showed a significant amount of noise that prevented the execution of a 400 V DC-bus test, and it is therefore only tested with a 200 V DC-bus. It is expected that small corrections would resolve the noise problem and enable the 9-phase PMSM to be driven on a 400 V DC-bus.

Acknowledgement

The authors of this work gratefully acknowledge Grundfos for sponsoring the 9th MechMan symposium.

References

[1] M. Zabaleta, E. Levi, and M. Jones, “Modelling approaches for triple three-phase permanent magnet machines,” in 2016 XXII International Conference on Electrical Machines (ICEM 2016).
[2] B. M. Wilamowski and J. D. Irwin, Power Electronic and Motor Drives. CRC Press.
[3] T. Frandsen, “Motor integrated permanent magnet gear,”
[4] T. Miller and M. McGilp, “Analysis of multi-phase permanent-magnet synchronous machines,” pp. 1–6, 2009.
[5] S.-H. Kim, Electrical Motor Control: DC, AC, and BLDC Motors. Elsevier Science Technology.